Dossier

This paper is a part of the hereunder thematic dossier published in OGST Journal, Vol. 67, No. 6, pp. 883-1039 and available online here

Cet article fait partie du dossier thématique ci-dessous publié dans la revue OGST, Vol. 67, n°6, pp. 883-1039 et téléchargeable ici

DOSSIER Edited by/Sous la direction de : **B. Bazin**

Challenges and New Approaches in EOR

Défis et nouvelles approches en EOR

Oil & Gas Science and Technology – Rev. IFP Energies nouvelles, Vol. 67 (2012), No. 6, pp. 883-1039

IFP Energies nouvelles

Oil & Gas Science and Technology – Rev. IFP Energies nouvelles, Vol. 67 (2012), No. 6, pp. 903-919

DOI: 10.2516/ogst/2012016

Dossier

Challenges and New Approaches in EOR
Défis et nouvelles approches en EOR

Hydrophobically Modified Sulfonated Polyacrylamides for IOR: Correlations between Associative Behavior and Injectivity in the Diluted Regime

G. Dupuis[1,2‡], D. Rousseau[1*], R. Tabary[1], J.-F. Argillier[1] and B. Grassl[2]

1 IFP Energies nouvelles, 1-4 avenue de Bois-Préau, 92852 Rueil-Malmaison Cedex - France
2 IPREM-EPCP / Université de Pau et des Pays de l'Adour, Hélioparc, 2 av. Pdt Angot, 64053 Pau cedex 09 - France
‡ Now with POWELTEC, 3 rue Paul Héroult, ZAC Rueil 2000, 92500 Rueil-Malmaison - France
e-mail: guillaume.dupuis@poweltec.com - david.rousseau@ifpen.fr - rene.tabary@ifpen.fr
jean-francois.argillier@ifpen.fr - bruno.grassl@univ-pau.fr

* Corresponding author

Résumé — Polyacrylamides sulfonés modifiés hydrophobes pour la RAH *(IOR)* : corrélations entre le caractère associatif et l'injectivité en régime dilué — Nous présentons de nouvelles corrélations expérimentales entre l'injectivité dans des membranes de polycarbonate et le caractère associatif de Polymères Hydrosolubles Modifiés Hydrophobes (PHMH) ayant des squelettes de polyacrylamide sulfoné (PAMS) et des compositions variables en unités hydrophobes. Cette étude concerne, d'une part, la caractérisation du caractère associatif des polymères en régime dilué et semi-dilué et d'autre part, leur injectivité lors de filtrations frontales en régime dilué. Les résultats de viscosimétrie et de diffusion dynamique de la lumière révèlent l'existence de seuils en termes de quantité (≥ 0,5 mol%) et de masse (≥ C12) des unités hydrophobes alkyles, au-delà desquels des interactions interchaînes apparaissent. Ces interactions se traduisent par la présence d'agrégats dans les solutions diluées et par un pouvoir épaississant nettement plus marqué des polymères dans les solutions semi-diluées.

L'étude de filtration a été effectuée sur des membranes à pores capillaires calibrés (membranes de type *track-etched*) dans le régime de Darcy à débit constant et à Jamming Ratio élevé. Les résultats montrent que :

– l'injection de solutions diluées de PHMH sans interactions interchaînes (*i.e.* avec des compositions en unités hydrophobes en-dessous des seuils indiqués ci-dessus) ne conduit pas à des réductions de mobilité et de perméabilité plus importantes que celles obtenues avec des polymères hydrosolubles de référence;
– l'injection de solutions diluées de PHMH avec des interactions interchaînes conduit à des réductions de mobilité et de perméabilité significatives;
– les réductions de mobilité et de perméabilité provoquées par les PHMH sont essentiellement dues à l'adsorption irréversible de polymère sur la paroi des pores et non à la formation de cakes de filtration;
– les épaisseurs des couches adsorbées de PHMH sont limitées par la contrainte effective appliquée par l'écoulement des solutions à travers les pores.

Abstract — Hydrophobically Modified Sulfonated Polyacrylamides for IOR: Correlations between Associative Behavior and Injectivity in the Diluted Regime — *We report new experimental correlations between the injectivity through polycarbonate membranes and associative properties of random Hydrophobically Modified Water Soluble Polymers (HMWSP) with sulfonated polyacrylamides (SPAM) backbones and variable compositions in hydrophobic units. The investigations are focused on both their associative behavior in the diluted and semi-diluted regime and their injectivity under frontal filtration conditions in the diluted regime. Results from viscosimetric and dynamic light scattering measurements indicate the existence of thresholds in terms of amount (≥ 0.5 mol%) and mass (≥ C12) of alkyl hydrophobic units above which interchain interactions arise. These interactions are evidenced by the presence of multichain aggregates in diluted solutions and by enhanced thickening abilities in semi-diluted solutions. The filtration study was performed with capillary pore membranes (track-etched) in the Darcy regime under constant-flow rate and high Jamming Ratio conditions. Results show that:*

- *injection of diluted solutions of HMWSP without interchain interactions (i.e. with composition in hydrophobic units below the above mentioned thresholds) does not lead to significant mobility and permeability reductions as compared to the injection of a reference Water Soluble Polymer (WSP);*
- *injection of diluted solutions of HMWSP with interchain interactions leads to significant mobility and permeability reductions;*
- *HMWSP-induced mobility and permeability reductions are essentially due to irreversible polymer adsorption on the pore walls and not to the formation of filter-cakes;*
- *HMWSP adsorbed layers thicknesses are limited by the effective stress applied by the solution's flow in the pores.*

NOMENCLATURE

Acronyms

AM	Acrylamide
AMPS	Sulfonated Acrylamide (Sodium-2-Acrylamido-2-Methylpropanesulfonate)
DLS	Dynamic Light Scattering
HMWSP	Hydrophobically Modified Water Soluble Polymer
IOR	Improved Oil Recovery
MALS	Multi Angle Light Scattering
MSEC	Micellar Size Exclusion Chromatography
RAH	Récupération Améliorée des Hydrocarbures
SEC	Size Exclusion Chromatography
SLS	Static Light Scattering
SPAM	Sulfonated Polyacrylamide
WSP	Water Soluble Polymer

Symbols

C	Polymer concentration (g/L)
C^*	Coil overlap concentration (g/L) (for non-associative polymers)
C_η	Viscosity upturn concentration (g/L) (for associative polymers)
d_h	Hydrodynamic diameter (μm)
I_P	Polydispersity index
Jr	Jamming ratio (pore diameter of the membrane divided by the hydrodynamic diameter of the polymers or the polymer aggregates)
k	Permeability (μm^2)
k_H	Huggins constant
k_i and k_f	Initial and final permeability of the membrane (μm^2)
k_P	Permeability of the membrane during polymer injection (μm^2)
L	Membrane thickness (μm)
l_{capi}	Length of the capillary tube (m)
M_W	Weight-average molar mass (g/mol)
Q	Injection flow rate (mL/h)
r_{capi}	Internal radius of the capillary tube (μm)
Rm	Mobility reduction (ΔP during polymer injection divided by reference ΔP)
Rk	Permeability reduction (ΔP after polymer injection divided by reference ΔP)
r_P	Pore radius of the membrane (μm)
V	Volume injected (mL)

Greek Symbols

α_{Irrev}	Irreversible permeability impairment
α_{Rev}	Reversible permeability impairment
ΔP	Pressure drop over the membrane
ΔP^{capi}	Pressure drop over the capillary tube
ε_h	Polymer adsorbed layer thickness (μm)
Φ	Porosity (%)
$\dot{\gamma}_{wall}$	Wall shear rate in the membrane's pores ($\dot{\gamma}_{wall}^{capi}$ in the capillary tube) (s^{-1})
$\dot{\gamma}_{wall}^{eff}$	Effective wall shear rate in the membrane's pores (s^{-1})
$[\eta]$	Intrinsic viscosity (mL/g)

η Viscosity of the effluent solution downstream the membrane (Pa.s)
η_B Brine viscosity (Pa.s)
η_P Viscosity of the injected polymer solution (Pa.s)
η_P^{app} Apparent viscosity of the polymer solution flowing through the membrane's pores
η_0 Polymer Newtonian viscosity (Pa.s)
η_{r0} Relative Newtonian viscosity

INTRODUCTION

Hydrophobically Modified Water Soluble Polymers (HMWSP) differ from classical Water Soluble Polymers (WSP) in that they are partially composed of hydrophobic monomers capable of creating micelle-like physical associations in solution. These nanostructures confer specific rheological and adsorption properties to HMWSP, making them, respectively, attractive for two different Improved Oil Recovery (IOR) applications [1-3]: mobility control (polymer flooding) and well treatments operations. However, controlling the flow of polymers solutions in porous media is a major concern and the classical models developed for WSP fail in the case of HMWSP, in particular because the injectivity of HMWSP solutions markedly depends on retention, adsorption and rheology. In this paper, we propose to correlate, for the first time, the associative behavior of new HMWSP to their injectivity in diluted regime through capillary pores membranes.

Numerous studies related to the association behavior of HMWSP in the diluted regime are reported in the literature. Various techniques have been implemented among which viscosimetry [4-12], fluorescence [13-16], transmission, scanning and environmental scanning electron microscopy (TEM, SEM and ESEM) [16-18], ^{19}F NMR spectroscopy [19, 20], neutron scattering [21-24] and Static and Dynamic Light Scattering (SLS and DLS) [14-16, 25-37]. Theoretical approaches have also been proposed to describe HMWSP static [38, 39] and dynamic [40] properties. Although intrachain associations are often reported as being dominant over interchain associations in the diluted regime, the conclusions of the different studies are largely dependent on the HMWSP microstructure, the chemical composition of the various constituents and the physicochemical conditions (salinity, pH and temperature).

Polymer solution flow in porous media is a broad topic which has been widely investigated for classical WSP. However, in their 2001 review, Chhabra *et al*. [41] pointed out the persistent lack of definitive and quantitative information available on the role of viscoelasticity and of the effects arising from polymer/wall interactions, polymer retention, etc. Accordingly, from the results of frontal filtration experiments involving non-diluted solutions of polyacrylamides, Surý and Machač [42] stress on the significant contribution of polymers viscoelasticity (due to extensional deformations) to the control of the filtration process. Regarding more specifically WSP flow in porous media in the Darcy regime and under constant flow rate conditions, comprehensive reviews have been carried out by Sorbie [43] and Chauveteau and Sorbie [44]. The impact of pore wall exclusion effects on the apparent viscosity [45, 46] and the coil-stretch transitions of adsorbed macromolecules in elongational flows [47] have been studied in details. More recent works have also suggested the existence of bridging adsorption phenomena [48] on the pore throats walls. Regarding HMWSP flow in porous media, much fewer references can be found, but the available results [49, 50] indicate significantly higher injection pressures for HMWSP than for corresponding WSP, which are attributed to higher adsorption for HMWSP. Such interpretations are consistent with HMWSP adsorption studies performed under static conditions, which have shown that adsorption isotherms do not tend to a plateau when increasing polymer concentration [51-53]. These results are classically interpreted by the formation of multilayers of adsorbed HMWSP due to hydrophobic interchain interactions. Publications on HMWSP membrane filtration are particularly scarce as, apart from investigations carried out under cross-flow conditions by Wakeman and Akay [54, 55], to our knowledge, only one frontal filtration study was performed, by Kun *et al*. [56], with HMWSP that were only partially characterized.

As a general outcome from the literature, it appears that correlating HMWSP properties in solution to mechanisms controlling their injectivity remains an issue. Indeed, regarding in particular the high HMWSP adsorption, the role played by microstructures in solution has never been assessed. We have performed a combined experimental study of both solution properties and injectivity behavior of HMWSP. We chose to focus on HMWSP based on sulfonated polyacrylamide (SPAM) copolymers. A consistent and well characterized set of SPAM-based HMWSP bearing randomly distributed sulfonated units and alkyl side-groups with variable sizes and molar fractions, together with a reference WSP *(Fig. 1)*, was synthesized by micellar copolymerization so as to obtain the same molar mass and molar mass distribution.

The molar mass determination involved in particular a newly-developed Micellar Size Exclusion Chromatography (MSEC) technique [57]. The associative behaviors in bulk solution were then examined by DLS and viscosimetry in terms of both hydrodynamic sizes and interchain interactions.

The injectivity study in the diluted regime was based on frontal filtration experiments carried out on polycarbonate membranes with calibrated capillary pores. The Jamming Ratio *(Jr)* could hence be relevantly estimated from the ratio of the pore diameter to the hydrodynamic sizes determined by DLS and was always such as $Jr > 1$ or $Jr \approx 1$. The relative contribution of mechanisms linked to steric effects and adsorption on the control of injectivity was directly assessed from both pressure drop measurements during injection and

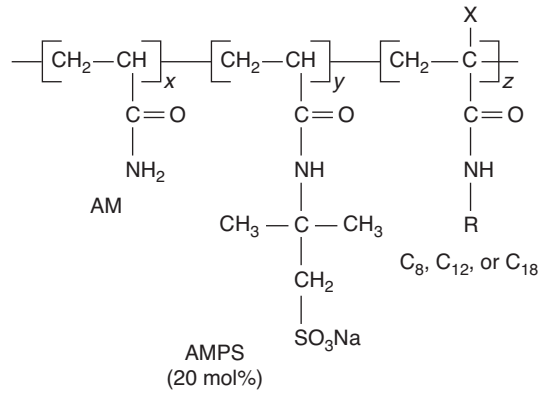

R	X	z (mol%)
C_8 : $C(CH_3)_2\ CH_2C(CH_3)_3$	H	0 or 0.5
C_{12}: $(CH_2)_{11}\ CH_3$	CH_3	0, 0.1, 0.2 or 0.5
C_{18}: $(CH_2)_{17}\ CH_3$	H	0 or 0.5

Figure 1

Chemical structure of the SPAM-based HMWSP and WSP (M_W = (1.2 ± 0.1).10^6 g.mol^{-1} and I_P = 1.8 ± 0.2). AM = Acrylamide; AMPS = Sodium-2-Acrylamido-2-Methylpropanesulfonate.

post-mortem SEM analysis. Adsorption isotherms were not determined because they imply adsorption under static conditions, which cannot easily be compared to adsorption from an HMWSP solution flowing though membrane pores. All membrane filtrations were performed at constant flow rate and in the Darcy regime. The study was carried out in two steps:

– successive filtrations of the same solution in different membranes, in order to propose a general microscopic interpretation of the mechanisms in play;
– investigations of the impact of flow rate, concentration and chemical composition, aimed at confirming and broadening the proposed interpretation.

1 MATERIALS AND METHODS

1.1 Synthesis and Characterization

This section summarizes our previous paper [57], in which we have presented the synthesis conditions and the chemical structure characterizations of the polymers. The polymers were prepared according to the micellar copolymerization method, reviewed by Candau and Selb [58], where the hydrophobic monomers are solubilized within surfactant micelles. The surfactant concentrations were adjusted to provide an average number of hydrophobic monomers per micelle N_H = 1 for each synthesis. Both HMWSP and WSP were synthesized in the same conditions, with differences lying only in the concentration and nature of the hydrophobic monomers. As shown in Figure 1, hydrophobic alkyl chains where either C12 at 0.1, 0.2 and 0.5 mol%, C8 at 0.5 mol% or C18 at 0.5 mol%. In the following, the reference non-hydrophobic polymer is named I20 and the HMWSP are named I20CH-Z. "I" refers to the ionic character of AMPS, "20" is the molar percent content of AMPS, "H" the number of carbons in the hydrophobic units and "Z" the molar percent content of hydrophobic units. Before use, the full set of polymers was fully characterized in terms of chemical composition by ^{1}H NMR analysis in D_2O (*Brucker* AVANCE 400 MHz) and molar mass distribution determination. Since the determination of the molar mass distribution of HMWSP by conventional Size Exclusion Chromatography (SEC) is generally difficult because of their strong adsorption, considered to lead to column plugging [59], we proposed an original method to determine the weight-average molar mass (M_W) and the polydispersity index (I_P) of the samples based on using surfactant. Further information concerning this method, called Micellar SEC, can be found in our previous paper [57].

1.2 Solution Preparation

All solutions were prepared in a "standard brine", composed of 20 g/L NaCl and 400 mg/L NaN_3 (used as a bactericide) in *Milli-Q*® water, filtered through 0.22 µm MF (cellulose esters) *Millipore*™ membranes. Stock polymer solutions were prepared by dissolution of a known amount of polymer powder in standard brine. After 72 hours of stirring, these solutions were allowed to stand for 7 days and their concentrations were verified by carbon analysis using a carbon analyzer (TOC-V_{CSN}) from *Shimadzu*. The stock solutions were stored at 4°C, over periods of time not exceeding 3 months. Prior to a given experiment, the final desired solution concentration was obtained by diluting the stock solution with the standard brine. Diluted solutions were allowed to stand during 24 hours for homogenization. Their concentrations were also checked by carbon analysis. Prior to the membrane filtration tests, all fluids were degassed under vacuum and kept under a helium cap during the experiments to prevent any bubble formation.

1.3 Solution Characterizations

Rheological measurements were conducted using a Low-Shear viscometer LS30 from *Contraves* equipped with a 2T-2T geometry for polymer concentrations below 2 g/L and a MCR300 rheometer from *Physica-Anton-Paar* fitted with a Mooney-Ewart geometry for higher concentrations. The shear rates investigated ranged from 1 to 130 s^{-1} with the LS30 and from 0.001 to 500 s^{-1} with the MCR300.

DLS measurements were performed using a Vasco-2 from *Cordouan Technologies*, working at a fixed back-scattering angle of 135° (λ = 658 nm). DLS technique, which is based on the fact that the Brownian motion of particles causes the light scattered from a dispersion to fluctuate over time, allows determining the hydrodynamic diameter d_h of dispersed particles, namely polymer molecules or polymeric aggregates [60]. The normalized time autocorrelation function of the scattered intensity $g^{(2)}(\tau)$ (τ being the delay time) is related to the electric field autocorrelation function $g^{(1)}(\tau)$ by a linear relationship (Siegert's relationship). If the size distribution of the dispersed particles is narrow, $g^{(1)}(\tau)$ presents an exponential decay with a decay rate Γ proportional to the z-averaged translational diffusion coefficient D_z of the diffusing particles. If the system is sufficiently diluted, the measured D_z represents a correct approximation of the translational diffusion coefficient at infinite dilution, $D_{z\infty}$ and the particles hydrodynamic diameter d_h is then given by the Stokes-Einstein equation. DLS can be used to identify well-separated bimodal size distribution but this technique does not easily allow computing size distributions of strongly polydisperse samples. Accordingly, in this paper, the DLS results are presented under the form of normalized $g^{(2)}(\tau)$ time autocorrelation functions, in order to allow a direct and satisfactorily comparison between the polymers studied. These curves were analyzed according to the Padé-Laplace algorithms implemented in the *Cordouan*'s software. Although this data analysis method can always provide numerical results, it appeared that the quantitative size determination results were reliable only when monomodal size distributions were found. All solution characterization experiments were carried out at 30°C.

2 MEMBRANE FILTRATION TESTS

2.1 Membrane Characteristics

All membrane filtration experiments were carried out on polycarbonate membranes from *SPI Pore*™, having calibrated capillary pores and a hydrophilic polyvinylpyrrolidone surface coating. These membranes are manufactured according to the "track-etched" process which allows getting well controlled capillary bundle morphology. Characteristics of the membranes used were as follows: porosity φ = 14.1%, pore diameter $2r_P$ = 2.6 μm (from SEM imaging) and thickness L = 9 μm.

The membranes, of net diameter d_m = 45 mm, were placed in a filtration cell (*Millipore*™) which was saturated under vacuum with standard brine. All membranes used in this work presented the same initial permeability:

$$k = (5.0 \pm 0.2) \cdot 10^{-3}\ \mu m^2$$

It is worth stressing here that the equivalent bundle of capillaries pore diameter that can be estimated from this permeability, $2r_{Pbc} = 2\sqrt{8\,k/\varphi}$, is different from the SEM radius ($2r_{Pbc} \approx 1.2$ μm). This is essentially due to the fact that:

- because of the manufacturing process, the pores are not perpendicular to the membrane's surface (the membranes can hence not be considered as bundles of capillaries);
- the manufacturer's porosity was not checked and could be rather overestimated.

2.2 Experimental Setup

The frontal filtration experimental setup consisted in:

- an injection system with two constant flow rate piston pumps for injecting brine (*Pharmacia* P-500) and polymer solutions (*Quizix* QX6000);
- the filtration cell (set horizontally in a 30°C-thermo-regulated bath);
- a calibrated capillary tube of internal diameter $2r_{capi}$ = 760 μm and length l_{capi} = 1 m (used to achieve a real-time estimation of the effluent polymer concentration from Poiseuille's viscosity measurements).

A bypass line enabled injecting either the brine alone or the polymer solution into either the filtration cell or the capillary tube. Differential pressure transducers from ABB linked to a data acquisition system enabled measurements of the pressure drops (ΔP) over the filtration cell and the capillary tube.

2.3 Experimental Procedure

The following experimental procedure was implemented:

- reference injection of the brine in both the membrane (ΔP_{Bi}) and the capillary tube (ΔP_{Bi}^{capi}) at the experiment's volumetric injection flow rate Q;
- injection of the polymer solution at Q in the capillary tube *via* the bypass line (ΔP_P^{capi});
- injection of the brine in both the membrane and the capillary tube at Q;
- injection of the polymer solution at Q in both the membrane (ΔP) and the capillary tube (ΔP^{capi});
- injection of the brine at Q in both the membrane (ΔP_{Bf}) and the capillary tube (ΔP_{Bf}^{capi}).

The pressure drops measured over the membrane were normalized and expressed in terms of mobility and permeability reductions, *Rm* and *Rk*, respectively defined, according to Darcy's law, as the ratios of pressure drops during and after polymer injection, to pressure drops before polymer injection:

$$Rm = \frac{\Delta P}{\Delta P_{Bi}} = \frac{\eta_P^{app}}{k_P} \times \frac{k_i}{\eta_B} \quad \text{and} \quad Rk = \frac{\Delta P_{Bf}}{\Delta P_{Bi}} = \frac{k_i}{k_f} \qquad (1)$$

where, η_P^{app} and η_B are, respectively, the apparent viscosity of the polymer solution flowing through the membrane pores

and the viscosity of the brine; and where k_i, k_P and k_f are, respectively, the initial permeability of the membrane, the permeability of the membrane during polymer injection and the final permeability of the membrane accounting for irreversible permeability modification.

The pressure drops measured over the capillary tube were used to determine the viscosity η of the effluent solution downstream the membrane during polymer injection, relative to the viscosity η_P of the injected polymer solution, according to Poiseuille's law: $\eta/\eta_P = \Delta P^{capi}/\Delta P_P^{capi}$. It should be stressed that the capillary tube was not subjected to irreversible permeability modification since, for all experiments, $\Delta P_{Bf}^{capi} = \Delta P_{Bi}^{capi}$.

Estimations of the wall shear rates in both the membrane's pores $\dot{\gamma}_{wall}$ and the capillary tube $\dot{\gamma}_{wall}^{capi}$ were performed by assuming parabolic velocity profiles [61]. This led to:

$$\dot{\gamma}_{wall} = \frac{4Q}{r_P \varphi S} \quad \text{and} \quad \dot{\gamma}_{wall}^{capi} = \frac{4Q}{\pi r_{capi}^3} \tag{2}$$

S being the effective filtration surface of the membrane (*i.e.* with a correction corresponding to the filter holder's surface). Within the range of flow rates investigated (Q = 2 to 500 mL/h), $\dot{\gamma}_{wall}$ varied from 15 to 3 800 s^{-1} but the corresponding Reynolds numbers (as calculated with a viscosity of 1.5 mPa.s, representative of the majority of this work's polymer solutions) remained low (Re ~ 10^{-4} to 10^{-3}), thanks to the large number of capillary pores. When adsorbed layer thicknesses were considered, effective wall shear rates, $\dot{\gamma}_{wall}^{eff}$, were calculated by taking into account both the reduction of the pores diameter and the reduction of the membrane's porosity. Such effective wall shear rates sometimes reached values above 10 000 s^{-1} but the Reynolds numbers were still kept to low values, namely Re < 10^{-2}. This means that flow over the membranes always corresponded to the Darcy (laminar) regime. Concerning the flow in the capillary tube, $\dot{\gamma}_{wall}^{capi}$ varied from 13 s^{-1} to 3 200 s^{-1} and the Reynolds number from Re ~ 0.6 to Re ~ 150. Thus, at high flow rate, inertial effects can play a role. As a consequence, since both entrance and inertial effects are known to significantly impair the determination of the Poiseuille's viscosity of a polymer solution [62], the on-line viscosity ratio η/η_P measured in our experiments could not strictly be assimilated to a polymer concentration ratio. Nevertheless, in the following, we do present plots of η/η_P because this parameter is relevant when it reaches a value close to 1, as it indicates that 100% of the injected polymer solutions viscosity is recovered downstream the membrane.

In addition to the on-line capillary measurements, complementary effluent characterizations have been carried out. For all experiments, Newtonian relative viscosity measurements, DLS measurements and carbon analysis were conducted on the injected solution and on the effluents samples collected at the beginning and at the end of the polymer injection. SEM images using a *Supra™* 40 from *Carl Zeiss* were also taken on dried membranes after completing the injection test and compared to a reference membrane exposed to brine only.

3 GENERAL CONSIDERATIONS ON FRONTAL FILTRATION

3.1 Microscopic Mechanisms

Pressure drop increases during constant flow rate frontal filtration of polymer solutions are due to both the apparent viscosity of the injected solution and to the permeability impairment of the membrane. Different microscopic mechanisms can be responsible for permeability impairments during filtration of solutes, particles and in particular, polymers. As reviewed, for example, by Van den Berg and Smolders [63], and depending of the Jamming Ratio, three main mechanisms can be identified:

– formation of an accumulation (or concentration polarization) layer above the surface of the membrane, which consists in a local increase of the polymer concentration upstream the membrane's surface and has been described for both

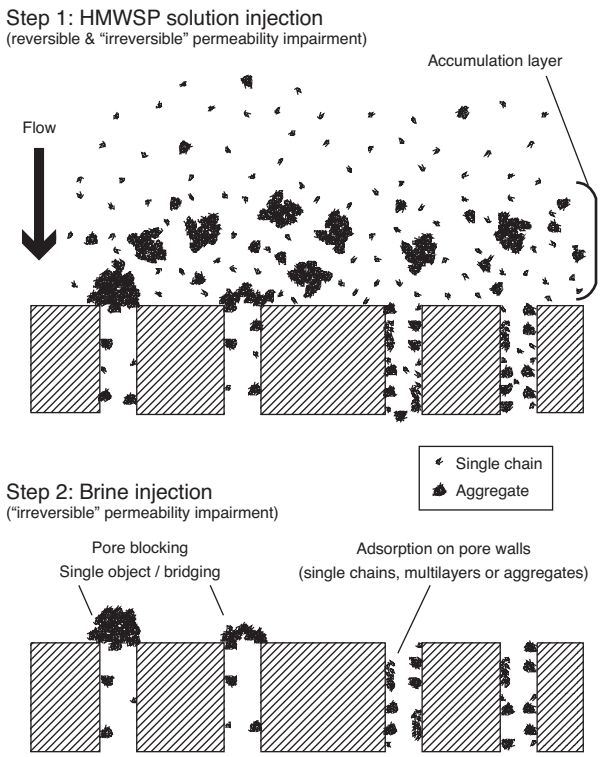

Figure 2

Schematic of the three main mechanisms potentially involved in HMWSP-induced permeability impairment (accumulation layer, pore blocking and adsorption on pore walls) of the membrane during the filtration of HMWSP, according to experimental procedure implemented.

cross-flow [63, 64] and frontal filtration [63, 65] geometries (applicable for $Jr < 1$ or $Jr \approx 1$);
- steric effect of pore blocking or bridging pore blocking (also applicable for $Jr < 1$ or $Jr \approx 1$);
- dynamic polymer adsorption on the membrane's pore walls, as described in particular by Bagassi *et al*. [47] on track-etched membranes (applicable for $Jr > 1$).

Manifestly, the first two mechanisms can lead to the formation of a filter-cake of polymer physical gel on the membrane surface. For HMWSP filtration, adsorption can also eventually entail filter-cake build-up, since it can involve multilayer adsorption through the formation of hydrophobic bonds between adsorbed chains [51].

The three mechanisms are schematically represented in Figure 2 for frontal filtration in a membrane with capillary pores. The schema is adapted to the case of HMWSP filtration (*i.e*., in particular, to the likely presence of interchain aggregates, as will be further discussed in this paper) and to the experimental procedure implemented in the present study, namely injection of the polymer solution (step 1), followed by injection of brine without polymer (step 2). This procedure allowed to check for both reversible permeability impairments, which take place only during the polymer solution injection and vanish during subsequent brine injection and irreversible permeability impairments, which prevail during long-term (on the experimental time scale, namely up to a few weeks) brine injections.

3.2 Useful Definitions

The concepts of mobility and permeability reductions (*Rm* and *Rk*) are particularly relevant for evaluating the effects of apparent viscosity and of both reversible and irreversible permeability impairments. In order to facilitate the discussion of the experimental results, we introduce α_{Irrev} and α_{Rev}, respectively the irreversible and the reversible permeability impairment coefficient defined as follows: $k_f = \alpha_{Irrev}\, k_i$ and $k_P = \alpha_{Rev}\alpha_{Irrev}\, k_i$. *Rm* and *Rk* can then be expressed as:

$$Rm = \frac{\eta_r^{app}(\dot{\gamma}_{wall}, depl)}{\alpha_{Rev}\alpha_{Irrev}} \approx \frac{\eta_{r0}}{\alpha_{Rev}\alpha_{Irrev}} \quad \text{and} \quad Rk = \frac{1}{\alpha_{Irrev}} \tag{3}$$

with η_r^{app} ($\dot{\gamma}_{wall}$, *depl*) and η_{r0} respectively the apparent relative viscosity and the bulk Newtonian relative viscosity of the polymer solution flowing through the membrane. Strictly speaking, the apparent relative viscosity depends not only on $\dot{\gamma}_{wall}$ but also on the presence of a depleted layer (noted "*depl*") [45, 46]. However:
- for the 6 polymers studied in this work, viscosimetric measurements performed in the diluted regime indicated only slight simple shear-thinning behavior;
- for diluted solutions, depletion layer effects can only entail a slight reduction of the apparent viscosity. Therefore, in the specific conditions of this study, the apparent relative viscosity can be considered as very close to the bulk Newtonian relative viscosity, η_{r0}.

When the permeability impairment is principally due to adsorption on the pore walls, the hydrodynamic thickness of the polymer adsorbed layer, ε_h, can be rather straightforwardly estimated from *Rk* and r_P by using Poiseuille's law:

$$\varepsilon_h = r_P \cdot (1 - Rk^{-1/4}) \tag{4}$$

r_P is preferred to r_{Pbc} here because it reflects the observed pore size of the membrane. ε_h should naturally be considered as a coarse estimation.

4 RESULTS AND DISCUSSION

4.1 Polymer Characteristics

^{1}H NMR molecular composition and MSEC-MALS characterization

According to previous works [66], careful ^{1}H NMR analysis in D_2O was used to ensure that the molar composition of the chains was as expected from the synthesis conditions and that the final purified products were free of unreacted monomers or surfactant molecules. Weight-average molar masses (M_W) and polydispersity index (I_P) determined by MSEC-MALS [57] are given in Table 1. According to the MSEC-MALS method, these data refer to intrinsic single chains properties, excluding the effects of hydrophobic bonds. Results show that all polymers (HMWSP and WSP) have nearly the same weight-average molar mass, $M_W = (1.2 \pm 0.1)\cdot 10^6$ g.mol^{-1} and polydispersity index, $I_P = 1.8 \pm 0.2$. These verifications were mandatory to allow performing a meaningful study of the influence of the nature and amount of hydrophobic monomers on HMWSP properties.

TABLE 1

Molecular and diluted solution properties of the polymers

Sample	M_W (10^6 g/L)*	I_P*	[η] (mL/g)	k_H	d_h (nm)
I20	1.3	1.8	560	0.4	100
I20C8-0.5	1.1	1.8	310	0.5	100
I20C12-0.1	1.3	1.7	520	0.5	120
I20C12-0.2	1.3	1.9	600	0.3	120
I20C12-0.5	1.3	1.8	500	0.5	*multimodal*
I20C18-0.5	1.1	1.6	510	1.7	*multimodal*

* Determined by MSEC (M_W and I_P refer to intrinsic chain properties, excluding the effects of hydrophobic bonds).

4.2 Associative Behavior in Solution

4.2.1 Diluted Solutions

Viscosimetric measurements

Results of intrinsic viscosity and Huggins constant determinations carried out in the standard brine are shown in Table 1. It appears that intrinsic viscosities are about the same for all polymers (namely $[\eta] = 550 \pm 50$ mL/g), except for I20C8-0.5 for which intrinsic viscosity is noticeably lower ($[\eta] = 310$ mL/g). As classically stated [67], for a given M_W, the intrinsic viscosity can be considered as proportional to the reciprocal of a "density in solution" of the polymers: the lesser $[\eta]$, the "denser", or the less swelled the polymers are. Lower $[\eta]$ for HMWSP as compared to WSP are often reported [7, 68] and attributed to the formation of intrachain bonds between hydrophobic units. Accordingly, our results suggest the presence of intrachain bonds in I20C8-0.5 solutions. Regarding the other HMWSP and particularly those with 0.5 mol% hydrophobic units (I20C12-0.5 and I20C18-0.5), the fact that their $[\eta]$ is close to that of I20 cannot be straightforwardly interpreted. Indeed, it could originate in compensation between intra and intermolecular links, resulting in macromolecular structures having comparable "densities in solution" as the reference WSP. DLS investigation will provide further insights to this regard. Huggins constant values of $k_H = 0.4 \pm 0.1$, characteristic of good solvent conditions, were obtained for both the reference polymer I20 and the HMWSP with C8 or C12 hydrophobic units. For I20C18-0.5, a k_H value above unity ($k_H = 1.7$) was obtained, indicating the existence of marked attractive interactions between the chains [69].

Dynamic Light Scattering

The concentration dependence of the DLS results within the diluted regime was investigated for all polymers. Figure 3 shows, as an example, the normalized $g^{(2)}(\tau)$ obtained for I20C12-0.5 in the standard brine at polymer concentrations of 0.5, 1 and 2 g/L (corresponding to the diluted regime, as will be shown in the next section). Since the curves are comparable, it appears that the hydrodynamic size of the polymeric particles does not depend on concentration between 0.5 and 2 g/L. Similar results were obtained in the same concentration range for all polymers, except for I20C18-0.5 for which concentration effects appeared at 2 g/L. In the following, we chose a polymer concentration of 1 g/L to provide a meaningful comparison between the polymers in the diluted regime.

The normalized $g^{(2)}(\tau)$ recorded for all polymers at 1 g/L are presented in Figure 4 and the hydrodynamic diameters, d_h, obtained from the analysis of the functions are reported in Table 1. It appears that the curves for I20, I20C8-0.5, I20C12-0.1 and I20C12-0.2 can almost be superimposed. For these samples, the data analysis indicated monomodal size distributions, with d_h close to 100 nm (the typical uncertainty range for DLS size measurements should be considered of about ± 30%). For I20C12-0.5 and I20C18-0.5, the normalized time autocorrelation curves are markedly different as for the other polymers and the data analysis revealed two decay modes (according to the Padé-Laplace analysis). Although in these cases a precise quantitative determination of the size was difficult, it appeared that the first decay mode was associated with sizes close to 100 nm, indicating the presence of isolated chains and the second corresponded to

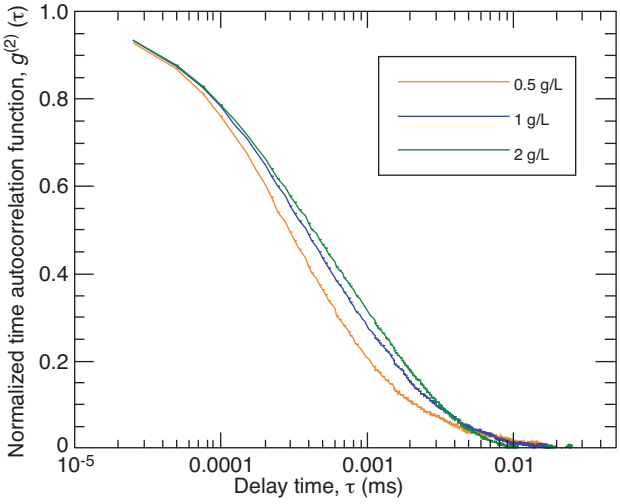

Figure 3

Normalized DLS time autocorrelation functions ($g^{(2)}(\tau)$) obtained with I20C12-0.5 at 0.5 g/L, 1 g/L and 2 g/L in standard brine.

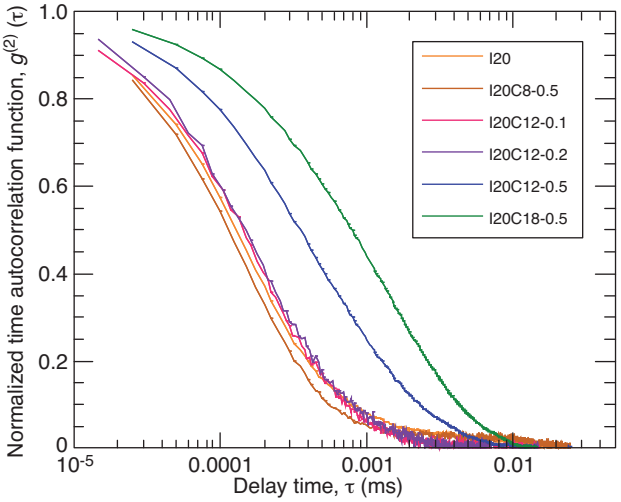

Figure 4

Normalized DLS time autocorrelation functions ($g^{(2)}(\tau)$) showing the impact of the chemical composition of the HMWSP compared to WSP. All measurements were carried out at 1 g/L polymer concentration.

sizes of the order of 1 000 nm, indicating the presence of multichain aggregates.

These results are consistent with DLS studies performed by other authors, in which two decay modes in diluted HMWSP solutions have also been reported and also associated to the presence of both single chain objects, with or without intramolecular hydrophobic bonds and multichain aggregates. This is in particular the case for Dai *et al*. [25-27] working on Hydrophobically modified Alkali Soluble Emulsions (HASE) made of random copolymers of methacrylic acid and ethyl acrylate with 1 mol% of various ethoxylated alkyl hydrophobic monomers, Sato *et al*. [15] working on random copolymers of acrylic acid and N-dodecylmethacrylamide at rather high molar fractions (5 to 30 mol%), Vidal *et al*. [35] working on carboxymethylcellulose modified with 1 to 6 mol% randomly distributed N,N-dihexylamine side-groups and Alami *et al*. [36], working on polyethylene oxyde end-capped with C12 chains. However, to our knowledge, DLS evidence of aggregates in diluted solutions of random HMWSP with SPAM backbones is reported here for the first time. Furthermore, DLS appears as an useful and time-saving method (as compared to fluorescence) to yield reliable estimates of HMWSP multichain aggregation before porous media experiments.

As general results from the diluted regime viscosimetry and DLS study it appears that:

– in diluted solutions, I20C8-0.5, I20C12-0.1 and I20C12-0.2 remain under the form of single chains with conformations close to that of the reference polymer I20. For I20C12-0.1 and I20C12-0.2, DLS size measurements are in agreement with the intrinsic viscosity results, indicating similar intrinsic viscosities for these two HMWSP and the reference polymer I20. For I20C8-0.5, a lower hydrodynamic size could have been expected from the lower intrinsic viscosity of this HMWSP. However, taking into account that d_h is proportional to $[\eta]^{1/3}$ at constant molar mass, the expected d_h of I20C8-0.5 could not have been lower than about 80 nm, namely a size that can not really be distinguished from 100 nm, considering the precision of DLS size measurements;
– multichain aggregates are present in diluted solutions of I20C12-0.5 and I20C18-0.5. According to the sizes associated to the second mode, these aggregates must involve up to a few chains. Nevertheless, since intrinsic viscosities of I20C12-0.5 and I20C18-0.5 are similar to that of I20, they must involve both intra and interchain bonds, in order to retain rather unchanged density in solution.

4.2.2 Thickening Ability of the Polymers

The concentration dependence of the Newtonian viscosity (η_0) of the solutions in standard brine at 30°C is shown in Figure 5. Since all polymers have similar molar mass, the results concerning the reference I20 polymer allow us to determine the coil overlap concentration, C^*, namely of about 2.1 g/L, which, as classically expected, is close to $[\eta]^{-1}$ ($[\eta]^{-1}$ = 1.8 g/L). For I20C8-0.5 and I20C12-0.1 and I20C12-0.2, no significant differences in viscosity are observed as compared to I20, except at very high polymer concentrations, above 20 g/L. When increasing the hydrophobic content of HMWSP up to 0.5 mol%, marked viscosity upturns occur at concentrations C_η close to C^*, as observed for I20C12-0.5 (C_η = 3.2 g/L) and I20C18-0.5 (C_η = 1.3 g/L). The critical concentration C_η is attributed to the formation of an intermolecular physical network by interchain interactions and can clearly be related to the presence of aggregates in diluted solutions of I20C12-0.5 and I20C18-0.5. For these HMWSP, the transition from diluted solutions to semi-diluted solutions could therefore be associated to a sol-gel transition controlled by a percolation mechanism [70]. However, DLS results below C_η do not show clear indication of an increase of the size of the aggregates when increasing the concentration. A detailed study of the properties of the solutions close to C_η would therefore be required to further understand the interchain aggregation mechanisms.

The major conclusion that can be drawn from our study of the bulk polymer-solvent properties is that the associative behavior of the HMWSP investigated can be discussed in terms of interchain interactions in both the diluted and the semi-diluted regimes. Accordingly, the results from viscosimetric and Dynamic Light Scattering measurements carried out on HMWSP with the same molar mass and molar mass distribution indicate the existence of thresholds in terms of amount (≥ 0.5 mol%) and mass (≥ C12) of alkyl hydrophobic

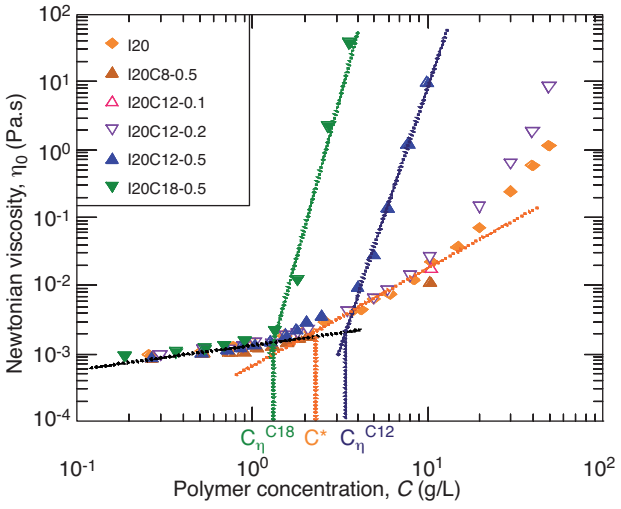

Figure 5

Newtonian viscosity (η_0) *vs* polymer concentration (C) for the 5 HMWSP investigated and the reference WSP. The straight lines allow estimating C^* and $C\eta$ (see text for definition).

units above which HMWSP enhanced interchain interactions take place and lead to multichain aggregates in the diluted regime and to enhanced thickening ability in the semi-diluted regime.

4.3 Frontal Filtration Experiments

4.3.1 Mechanisms Involved during Frontal Filtration of Diluted HMWSP Solutions

The objective of this part of the study was to determine the relative contribution of the different mechanisms involved in the frontal filtration of diluted HMWSP solutions. The option consisting in limiting the investigation to the diluted regime allows uncoupling the specific rheological properties of HMWSP from their other properties, in particular their adsorption. However, studying highly diluted solutions would not have been practical since their viscosities would have been difficult to distinguish from the solvent viscosity and since very large injection volumes would have been required to allow assessing for the final trends of the pressure curves. Accordingly the concentrations investigated were chosen relatively close to C^*, namely from 0.5 to 2 g/L. The corresponding relative viscosities were of the order of magnitude of 2. This means that viscosity effects could not entail by themselves mobility reductions above about 2.

The results presented in this section concern I20C12-0.5, which is a representative sample of HMWSP because it shows enhanced thickening ability and exhibit interchain interactions in its diluted solutions. In the following, the investigation consisting in successive injections of the same solution in distinct membranes at the same flow rate is presented first. The impacts of flow rate and of solution concentration (in the diluted regime) are addressed in a second step.

General results from effluent analysis

In order to assess for both transitory and stabilized filtration regimes, large volumes of typically 2 L of solution were injected during each filtration tests, which represents about 10^6 times the pore volume of the membranes. For all experiments it appeared that, after a very short transition period (less than 50 mL of solution injected), the concentration and the properties of the effluents were the same as the ones of the injected solution. More precisely, results indicated that:

- relative effluent viscosities η/η_P estimated from the capillary tube measurements reached the stable value of $\eta/\eta_P = 1$;
- Newtonian viscosities of collected effluent samples were identical to the initial viscosities within the uncertainty range of the viscometer;
- polymer concentrations in the effluent samples from carbon analysis were equal to the concentration of the injected solutions within the uncertainty range of the carbon analyzer;
- DLS $g^{(2)}(\tau)$ correlograms obtained from both injected solution and effluent were identical. In addition, for some experiments, collected effluents were also precipitated in ethanol, dried and used to prepare new solutions for viscosity measurements, ^{1}H NMR and MSEC-MALS analysis. These analyses revealed unchanged thickening abilities and molecular structures for the polymers in the effluents as compared to the polymers before any filtration.

Hence, as a general result, the amounts of injected solution were not sufficient to entail complete membrane plugging, neither mechanical degradation, nor conformation modification of the polymer chains flowing through the membranes. As a consequence, successive membrane filtration tests based on collected effluents could rightfully be considered as being performed with the *same solution* in terms of composition in solubilized HMWSP.

Successive membrane filtrations

The experiments described in this section were performed at a fixed flow rate Q of 500 mL/h (initial wall shear rate in the membrane's pore $\dot{\gamma}_{wall}$ = 3 800 s^{-1}) and at a fixed polymer concentration C = 1 g/L (η_{r0} = 1.7). Figure 6 shows Rm curves and the capillary tube's relative viscosity, η/η_P *versus* the injected volume (V) for three successive injections of the same solution of I20C12-0.5 in three different membranes. Table 2 shows the Newtonian viscosities and concentrations (determined by carbon analysis) of the injected solutions and of the effluent samples collected respectively at the beginning (after about 200 mL of solution injected) and at the end of each test as well a the Rm/η_{r0} values determined at the end of the polymer injections (for the 2nd and 3rd filtrations,

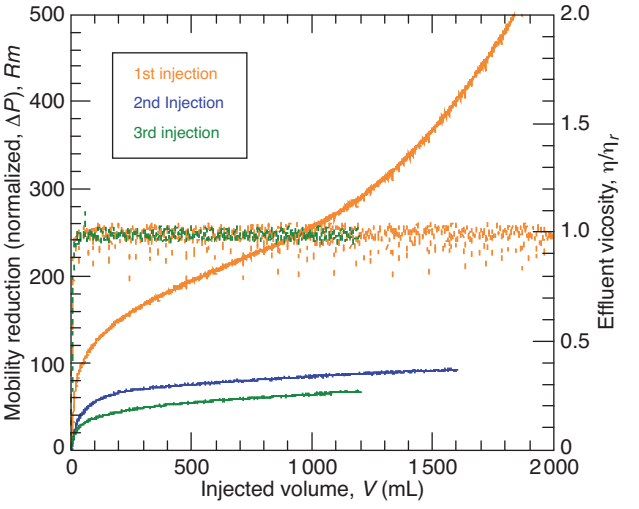

Figure 6

Successive frontal filtration of the same I20C12-0.5 solution in three different membranes – Rm curves (lines) and η/η_P (dots) from on-line capillary tube measurements; C = 1 g/L, Q = 500 mL/h. The stabilization trend observed from the 2nd filtration is typical of all HMWSP and WSP investigated in this study.

TABLE 2

Concentration by carbon analysis and viscosity determined before and during the three successive frontal filtrations of the same I20C12-0.5 solution; Rm/η_{r0} determined at the end of the polymer injections (extrapolated plateau values for the 2nd and 3rd filtrations) and stabilized *Rk* determined during the subsequent brine injections

	1st filtration			2nd filtration			3rd filtration		
	Inj. Sol.	1st Sampl.	2nd Sampl.	Inj. Sol.	1st Sampl.	2nd Sampl.	Inj. Sol.	1st Sampl.	2nd Sampl.
C (g/L)	1.00	0.99	0.94	0.97	0.97	0.99	0.98	1.02	0.98
η_{r0}	1.74	1.73	1.75	1.74	1.75	1.75	1.74	1.72	1.73
Rm/η_{r0}	546			57			40		
Rk	400			30			25		

these are extrapolated plateau values) and the stabilized *Rk* values determined during the subsequent brine injections.

As a first striking observation, the plots of Figure 6 indicate that the *Rm* values reached during the 3 tests are between 2 and 3 orders of magnitude above η_{r0}. Thus, obviously, marked permeability impairments of the membranes occur. Their origin will be discussed below, but it should be noted at this point that they must involve rather low amounts of polymers. Indeed, as indicated from the η/η_P values in Figure 6 and effluent analysis results presented in Table 2, after less than 100 mL of solution injected, the effluents present the same soluble polymer composition as the injected solution.

The second major observation concerns the marked difference in the *Rm* data between the 1st filtration on one hand and the 2nd and 3rd filtration on the other hand. During the 1st filtration, the shape of the curve suggests the superposition of two effects:

– a first increase limited by a plateau-like trend up to about 700 mL of polymer injected;
– a diverging trend beyond 700 mL of polymer injected. During the 2nd and 3rd filtrations, a sole plateau-like trend is observed, with much lower *Rm* values, although still significant as compared to the viscosity of the injected solution. Furthermore, passed the 1st filtration, the *Rm* values can be considered of the same order of magnitude.

The diverging trend observed during the 1st filtration is typical of the formation of an accumulation layer or of pore-blocking due to large and non-deformable objects that could be non-polymeric impurities or unswollen polymeric materials. Such impurities are frequently present in unfiltered polymer solutions. Indeed, as a result, the same diverging trend was observed during 1st filtrations of reference WSP solutions. SEM observation of the membrane after the 1st filtration is shown in Figure 7b and confirms this hypothesis as it clearly indicates a plugging of many pores by large objects, which can be the consequence of pore blocking either during the polymer injection, or during the subsequent water injection due to the previous formation of an accumulation layer. Accordingly, if larger volumes had been injected, the polymer concentration in the effluent would undoubtedly have dropped down. Conversely, SEM observation of the membrane after the 2nd filtration at the same magnification does not show plugging *(Fig. 7c)* as compared to the reference membrane *(Fig. 7a)*. Thus, in the following, we will focus on the understanding of the filtration mechanisms in play after having performed a 1st filtration, to assess solely for the intrinsic HMWSP properties in diluted solutions.

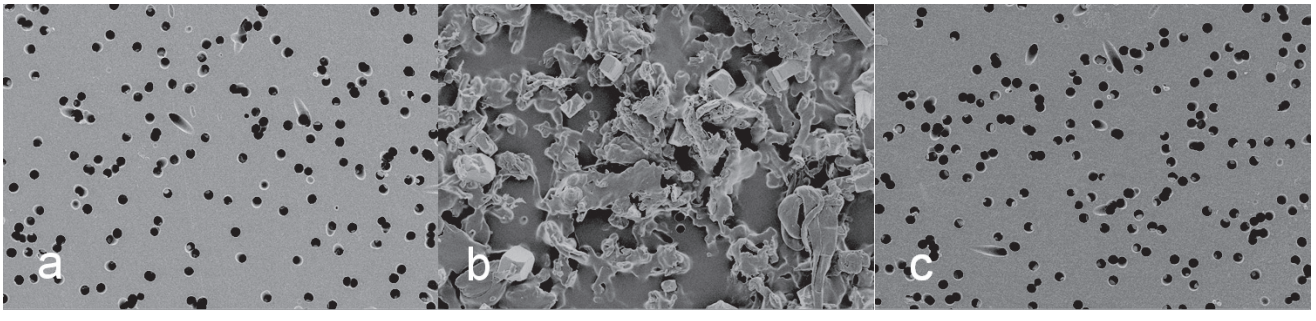

Figure 7

SEM images of a reference membrane dried a) after having been exposed to standard brine, b) of dried membranes after the 1st c) and the 2nd filtration of the same solution of I20C12-0.5 at C = 1 g/L and Q = 500 mL/h. Magnification × 1 000. Average pore diameter is 2.6 μm.

Restricting the discussion to the information provided by both the 2nd and 3rd filtration *Rm* curve in Figure 6 showing a stabilization trend and the SEM image of Figure 7c showing that only a low amount of polymer is retained is obviously not satisfactorily. Indeed, from these results, the permeability reduction could be due to both reversible and irreversible effects. In addition, irreversible effects could themselves be due either to soft pore blocking (involving deformable polymeric aggregates that could be expelled downstream the membrane when pressure is high enough, thus leading to a pressure-stabilized mechanism) or to adsorption on the pore walls. In Figure 8, we have plotted the data presented in the last two lines of Table 2, namely Rm/η_{r0} and *Rk versus* the injection number, respectively after the maximum volume injected for the 1st injection (about 2500 mL) and calculated from extrapolated normalized ΔP plateau values for the 2nd and 3rd filtrations. Since $Rm/\eta_{r0} \approx 1/(\alpha_{Rev}\alpha_{Irrev})$ and $Rk = 1/\alpha_{Irrev}$, these plots allow estimating the relative contribution of reversible and irreversible permeability reduction, irrespective of direct viscosity effects. The main result is that, for the 2nd and 3rd filtrations, $1/\alpha_{Irrev}$ appears to be much higher than $1/\alpha_{Rev}$. Indeed, for the 2nd and 3rd injections, $1/(\alpha_{Rev}\alpha_{Irrev}) \approx 60$ and 45, respectively, whereas $1/\alpha_{Irrev} \approx 30$ and 25. This means that the irreversible effects are responsible for a 25 to 30-fold reduction of the permeability of the membrane, while by taking into account the reversible effects, this permeability reduction is increased by only about 2-fold more. Thus, as a result, irreversible effects appear to be the dominant mechanisms controlling the permeability reduction of the membranes.

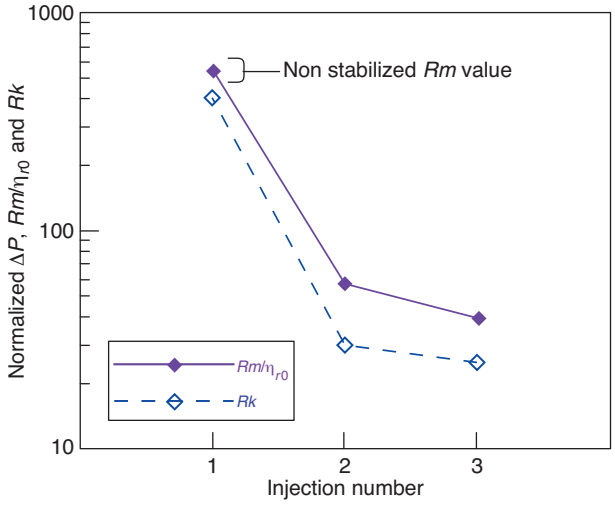

Figure 8

Normalized pressure drops, Rm/η_{r0} (◆) and *Rk* (◇), determined for the 3 successive filtrations of the same solution of I20C12-0.5 in 3 different membranes. Values for the 1st filtration were determined at the maximum volume injected (about 2 500 mL), values for the 2nd and 3rd filtrations correspond to extrapolated plateau values; C = 1 g/L, Q = 500 mL/h.

Figure 8 also show discrepancies between the results of the 2nd and the 3rd filtrations. Since no difference in terms of polymer concentration and viscosity are observed in the solutions used for the 2nd and 3rd filtrations *(Tab. 2)*, these discrepancies seem to be due to residual impurities remaining in the solutions after the 1st filtration. Accordingly, if more successive filtrations could had been performed, results would have converged to the same limiting Rm/η_{r0} and *Rk* values. However, in order to ensure reasonable experiment durations, only two successive membrane injections were performed in most of the tests presented in this paper. In the following, we will restrict the discussion to 2nd filtration results.

Estimating the relative contribution of soft pore blocking and adsorption on pore walls was made possible by examining the membrane by SEM at larger magnifications. The corresponding images, presented as comparisons between a reference membrane previously exposed to the standard brine and a membrane after a 2nd filtration of I20C12-0.5, are presented in Figure 9. From these pictures, NaCl crystals resulting of the drying of the brine can clearly be observed inside the pores. The pictures reveal no indication of pore-blocking objects. Conversely, evidences of polymer adsorbed on the pore walls can be seen, especially from the observation of the shape of the NaCl crystals which appear to be covered with dried polymer as well as from the observation of the bases of these crystals at the higher magnification level (× 100 000, images *Fig. 9g vs Fig. 9h*). Indeed, since membranes are extensively swept with brine after polymer injection, there cannot be free polymer remaining in the brine at the beginning of the drying process. Consequently, polymer cannot precipitate during drying and the only polymer material that is seen covering the NaCl crystals must be a polymer that has been adsorbed during the polymer injection. Such observations clearly indicate that HMWSP adsorption on pore walls is the main mechanism responsible for irreversible permeability reductions. Similar results have been obtained for the other HMWSP and the reference WSP investigated in this study. Furthermore, in a separated study, we have performed HMWSP injectivity tests in porous cores. The corresponding results, which are reported in a separated paper [71], are clearly consistent with an in-depth propagation of the polymers essentially controlled by adsorption on pore-walls.

As a consequence, in the sensitivity tests presented below, the *Rk* values will be used to calculate thicknesses of polymer adsorbed layers on the pore walls *(see Eq. 4)*. Theses thicknesses should however be considered as estimations, since a minor contribution of soft pore blocking to the irreversible permeability reduction cannot be excluded.

Impact of the injection flow rate

All results shown from this section were obtained after having performed a preliminary 1st filtration at Q = 500 mL/h.

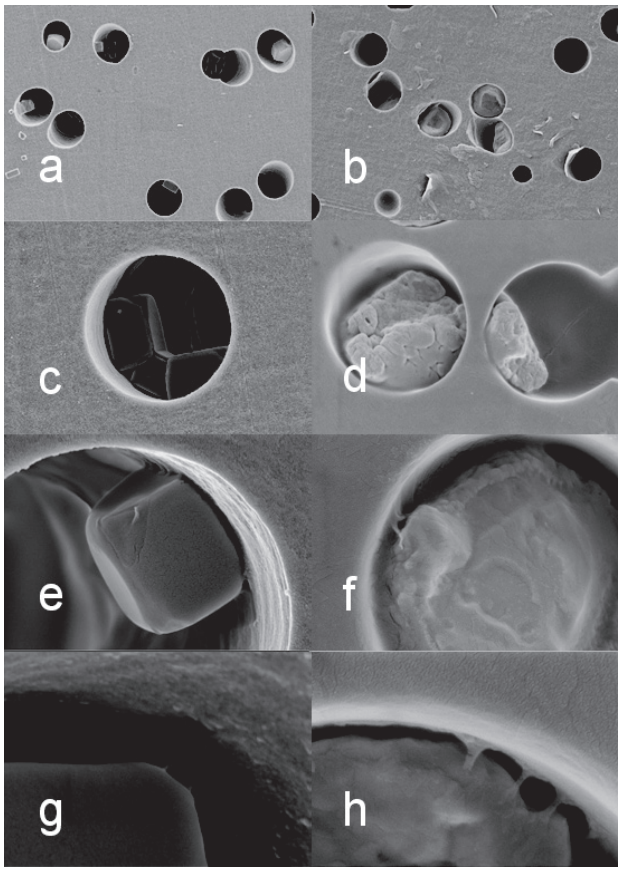

Figure 9

SEM images comparing a dry reference membrane previously exposed to standard brine (images a, c, e and g) and a dry membrane after the 2nd filtration of a solution of I20C12-0.5 at C = 1 g/L and Q = 500 mL/h (images b, d, f and h). Magnifications: × 5 000 (a, b), × 20 000 (c, d), × 50 000 (e, f) and × 100 000 (g, h). Average pore diameter is 2.6 µm.

In Figure 10 are shown the extrapolated plateau values of Rm/η_{r0} and Rk determined during the 2nd filtrations of C = 1 g/L solutions of I20C12-0.5 at flow rates ranging from 2 to 500 mL/h, corresponding to initial wall shear rates $\dot{\gamma}_{wall}$ ranging from 15 to 3 800 s^{-1}. Estimations of the polymer adsorbed layer thicknesses, ε_h, calculated from the Rk values are also presented.

As a first relevant observation from these results, it appears that permeability reduction during HMWSP injection is mainly due to irreversible effects (namely permeability reduction effects that persists after the water injection). Indeed, similarly as described in the previous section, Rm/η_{r0} and Rk at each flow rate are of the same order of magnitude, whereas Rk values indicate from 30-fold to 950-fold permeability reductions due to irreversible effects. It is also worth noticing that the ratio Rm/η_{r0} to Rk, which is an estimate of the reversible permeability reduction effects ($Rm/(\eta_{r0}Rk) = 1/\alpha_{Rev}$, *see Eq. 3*) decreases from ~ 4 to ~ 1.5 when the flow rate is increased from 2 to 500 mL/h. This variation, which is qualitatively consistent with a shear thinning of the solution flowing through the pores, can provisionally be considered as linked to a second order mechanism, with respect to the main aspects under discussion in this paper. Accordingly, in the following, we propose to discuss only the irreversible permeability reduction effects.

Results indicate a marked increase of Rk when reducing flow rate from 500 to 50 mL/h and a more moderate increase, possibly indicating a stabilization trend, from 50 to 2 mL/h. At the lower flow rates, the estimated layer thicknesses reach quite high values as compared to the pore radius (r_P = 1.3 µm). For example, at 2 mL/h, $\varepsilon_h \approx 1.07$ µm: this means that an open diameter of only about 0.4 µm remains for the flow of the solution inside each pore and that the effective final wall shear rate could be $\dot{\gamma}_{wall}^{eff} = 4\,200\ s^{-1}$ *i.e.* more than two orders of magnitude above the initial value of $\dot{\gamma}_{wall} = 15\ s^{-1}$. Nevertheless, we have already indicated that, for all experiments, both effluent analysis and plateau trends on the Rm curves clearly showed that no plugging of the membranes occurred. This is naturally consistent with the fact that Rk seems to tend to a limiting value and to this regard, the effective wall shear rate clearly appears as the stabilizing parameter. However it is not possible at this point to determine if the effective wall shear rate limits the transport of the polymeric particles toward the pore walls or if the thickness of the adsorbed layer is limited by the increase of the stress applied by the solution's flow.

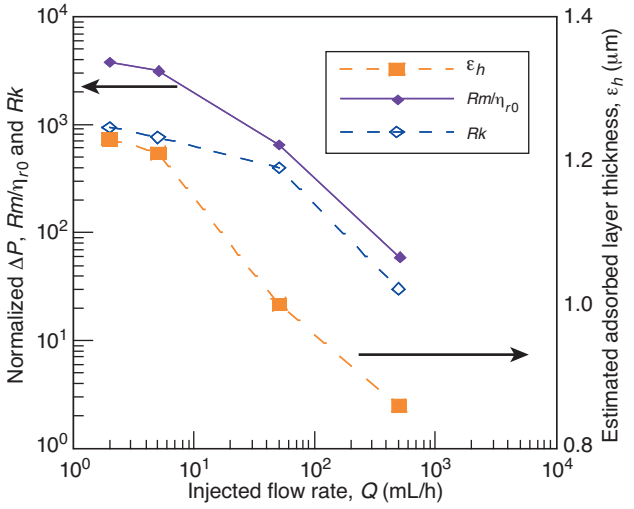

Figure 10

Normalized ΔP plateau values, Rm/η_{r0} (◆) and Rk (◇) (left axis), and polymer adsorbed layer thickness estimations, ε_h (■) (right axis), determined during the 2nd filtrations of 1 g/L solutions of I20C12-0.5 at flow rates ranging from 2 to 500 mL/h, corresponding to initial wall shear rates $\dot{\gamma}_{wall}$ ranging from 15 to 3 800 s^{-1}.

To address the latter question, the rheological behavior of the adsorbed layer formed during I20C12-0.5 injection at 5 mL/h was investigated by exposing it to brine flow rates of 5, 50 and 500 mL/h and then to 50 and 5 mL/h. Results are shown in Figure 11, in terms of estimated adsorbed layer thickness (ε_h) *versus* the effective final wall shear rates ($\dot{\gamma}_{wall}^{eff}$). All ε_h values were estimated from stabilized ΔP values. The results clearly show a shear-thinning behavior of the adsorbed layer when increasing shear rate. This shows that the main parameter limiting the adsorbed layer thickness is the stress applied by the solution's flow. The results also indicate that the adsorbed layers exhibit no shear-thickening behavior. This is consistent with the work of Bagassi *et al*. [47] since, on capillary pores polycarbonate membranes, elongational deformations are not significant enough to affect polyacrylamide-based polymers. In addition, considering that the thick HMWSP adsorbed layers are likely to be made of polymeric physical gels helps understanding why some hysteresis is observed when decreasing the flow rate. Indeed, the modification of the adsorbed layer's conformation when increasing flow rate can entail the formation of additional hydrophobic bonds between the adsorbed chains, which are not disrupted when decreasing the flow rate. A gel-like structure of the adsorbed layer might also be the reason why no single limiting value of the effective wall shear rate is found for the different experiments: the number of hydrophobic bonds inside the adsorbed layer and thus the physical gel's elasticity, is likely depending on the initial shear rate applied and the limiting stresses must be different for physical gel adsorbed layers with different elasticity.

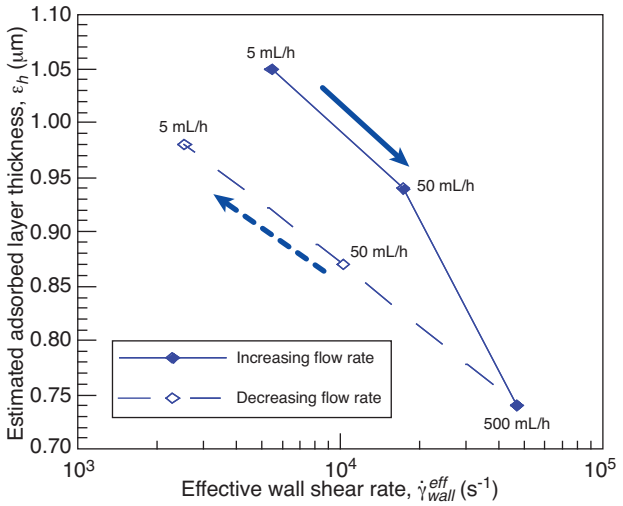

Figure 11

Estimated adsorbed layer thickness (ε_h) *versus* the effective wall shear rates ($\dot{\gamma}_{wall}^{eff}$) determined by exposing the adsorbed layer (formed during the injection of I20C12-0.5 at 5 mL/h) to brine flow rates ranging from 5 to 500 mL/h (◆) and then to flow rates ranging from 500 to 5 mL/h (◇).

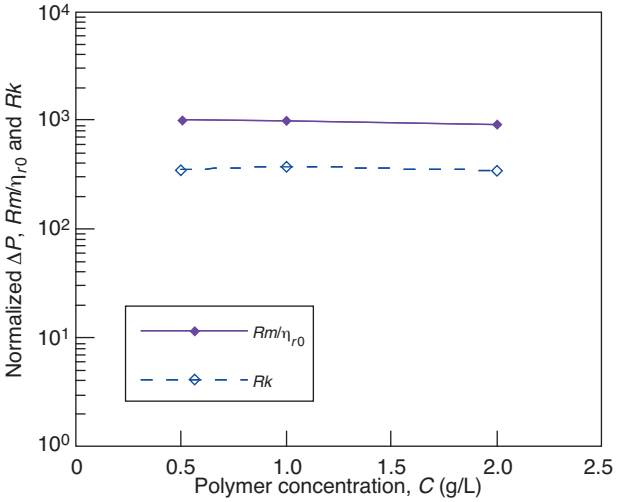

Figure 12

Impact of the concentration in the diluted regime: Rm/η_{r0} (◆) and Rk (◇) determined from plateau values for the second filtrations at Q = 50 mL/h of solutions of I20C12-0.5.

Impact of concentration in the diluted regime

The impact of concentration within the limits of the diluted regime was assessed as a complementary investigation. It was principally aimed at checking for possible soft pore-blocking due to the formation of interparticle bridges, which is a strongly concentration-dependent mechanism. Three sets of filtration tests were performed with solutions of I20C12-0.5 at C = 0.5, 1 and 2 g/L at Q = 50 mL/h corresponding to an initial wall shear rate, $\dot{\gamma}_{wall}$ = 380 s^{-1}. Stabilization trends were observed on the *Rm* curves for all 2nd filtrations and extrapolated plateau values of both *Rm* and *Rk* were determined. Results showing extrapolated plateau values of Rm/η_{r0} and *Rk versus* concentration are presented in Figure 12. As in the preceding sections, it appears that, for the 3 concentrations investigated, the permeability reductions are essentially due to irreversible effects. Furthermore, both Rm/η_{r0} and *Rk* values clearly show no concentration dependence. Therefore, soft pore blocking due to the formation of interparticle bridges can safely be neglected in the diluted regime.

4.3.2 Impact of the Chemical Composition

The impact of the chemical composition of the polymers was studied by performing comparative frontal filtration tests. For all polymers, the effluent analysis gave the same results as for I20C12-0.5: after only about 50 mL injected, the effluent compositions were identical to those of the injected solutions. In addition, during the 2nd filtrations, stabilization trends were always observed on the *Rm* curves *versus* injected volume. In Figure 13 are shown the extrapolated plateau values of *Rk* as well as the estimated adsorbed layer thicknesses (ε_h)

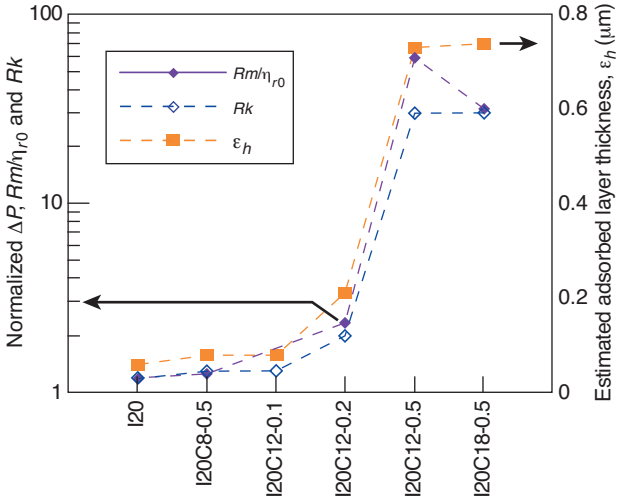

Figure 13

Impact of the chemical composition: normalized Δ*P* plateau values, Rm/η_{r0} (◆) and *Rk* (◇) (left axis) and polymer adsorbed layer thickness estimations, ε_h (■) (right axis), determined for the 2nd filtrations of the full set of polymers injected at C = 1 g/L and Q = 500 mL/h. Discontinuous junctions between dots are guides for the eyes.

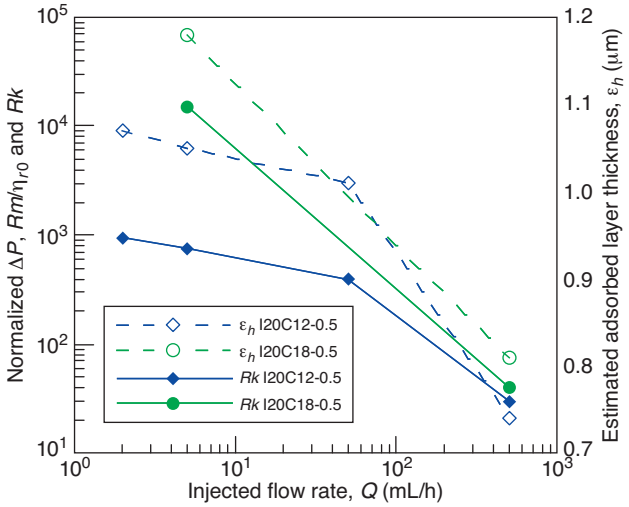

Figure 14

Impact of the chemical composition for different flow rates: extrapolated plateau values of *Rk* (filled symbols) and ε_h (open symbols) values determined during 2nd filtrations of I20C12-0.5 (◆ and ◇) and I20C18-0.5 (◆ and ◇) at 1 g/L and flow rates ranging from Q = 2 mL/h to Q = 500 mL/h. Lines are guides for the eyes.

determined during the 2nd filtrations of C = 1 g/L solutions of all polymers at Q = 500 mL/h (corresponding to $\dot{\gamma}_{wall}$ = 3800 s^{-1}).

As Rm/η_{r0} and *Rk* are of the same order of magnitude for the 5 HMWSP and the reference WSP, permeability reductions are always dominated by irreversible effects. It also appears that reversible effects are much less significant for I20C18-0.5 than for I20C12-0.5. This particular result must be linked to the specific structure of the C18 hydrophobic unit and would require complementary investigations. Although SEM analysis could not be systematically performed, it is reasonable to assume that, in all cases, irreversible permeability reduction effects were mainly due to polymer adsorption on the pore walls. Accordingly, in the following, the results will be discussed in terms of adsorbed layer thicknesses.

It also appears that only I20C12-0.5 and I20C18-0.5, namely the polymers which exhibit aggregates in their diluted solutions as well as enhanced thickening ability, entail irreversible permeability reductions above 10. For the 4 other polymers, the extrapolated *Rk* range between 1.2 and 1.9 correspond to ε_h from 0.06 μm to 0.19 μm. For I20C8-0.5 and I20C12-0.1, the ε_h values (ε_h = 0.08 μm) are close to those obtained for I20 (ε_h = 0.06 μm) and are of the order of magnitude of the hydrodynamic sizes obtained from DLS, namely d_h = 0.10 to 0.12 μm. This indicates that these 3 polymers were adsorbed as classical monolayers. This is also consistent with the fact that the DLS measurements showed no significant difference between I20, I20C8-0.5 and I20C12-0.1. For I20C12-0.2, the ε_h value (ε_h = 0.19 μm) is higher than the size in solution of the chains measured by DLS. This means that the dynamic adsorption behavior of this polymer reveals a slight ability for interchain aggregation. Nevertheless, in terms of substantial irreversible permeability impairment effects, the results shown in Figure 13 are consistent with the thresholds in terms of amount (≥ 0.5 mol%) and mass (≥ C12) of alkyl hydrophobic units identified in the study of the bulk polymer-solvent properties.

However, the similar ε_h values obtained for both I20C12-0.5 and I20C18-0.5 (respectively ε_h = 0.74 μm and ε_h = 0.81 μm) could be surprising considering the much higher thickening ability of I20C18-0.5. We have further investigated this issue by performing membrane filtrations of I20C18-0.5 at lower flow rate (Q = 5 mL/h; $\dot{\gamma}_{wall}$ = 38 s^{-1}). The corresponding results are shown in Figure 14 together with those obtained at 500 mL/h with I20C18-0.5 and those obtained with I20C12-0.5 at various flow rates, already presented in Figure 10. The results clearly show that, at Q = 5 mL/h, *Rk* and ε_h values are significantly higher for I20C18-0.5 than for I20C12-0.5. The irreversible permeability reductions obtained from low shear rate injections are thus consistent with the respective thickening abilities of I20C18-0.5 and I20C12-0.5, as determined from zero-shear viscosities. At higher shear rate, the fact that both polymers entail similar permeability reductions indicates that hydrophobic bonds are partly disrupted, as expected from their viscosimetric flow curves (not presented in this paper).

CONCLUSION

We have performed a detailed investigation of the solution properties and the injectivity behavior in the diluted regime of a set of SPAM-based Hydrophobically Modified Water Soluble Polymers (HMWSP). Viscosimetric measurements have evidenced the existence of thresholds in terms of amount (≥ 0.5 mol%) and mass (≥ C12) of the alkyl hydrophobic units to entail enhanced thickening ability as compared to a reference WSP. Moreover, DLS results have shown that diluted solutions of HMWSP with enhanced thickening ability contain multichain aggregates. Frontal membrane filtration tests performed in the Darcy regime with Jamming Ratio $Jr > 1$ or $Jr \approx 1$ have principally shown that:

– injection of HMWSP with enhanced thickening ability leads to marked permeability reductions;
– HMWSP injection does not entail plugging since the polymer concentrations downstream and upstream the membranes remain the same and the pressure curves show stabilization trends;
– permeability reductions are principally due to irreversible adsorption of the polymers on the membrane's pore walls;
– HMWSP adsorbed layers thicknesses are limited by the effective stress applied by the solution's flow in the pores of the membranes.

These experimental results allow understanding the dynamics of HMWSP-induced membrane permeability reduction. However, they do not allow to directly assess the microscopic mechanisms in play. Indeed, it is not possible at this point to determine whether the adsorbed layers are due to multichain aggregates adsorption and/or formation of multi-layers of single chains. Nevertheless, these results could be considered as a first step toward the modeling of HMWSP injectivity, which is a crucial parameter to control for IOR applications. Future works will naturally focus on investigating HMWSP injectivity in the semi-diluted regime.

ACKNOWLEDGMENTS

The "Association Nationale de la Recherche et de la Technologie" (ANRT) is acknowledged for a CIFRE PhD grant to Guillaume Dupuis. We also thank Didier Frot for his help in interpreting the DLS results, Nicolas Brodusch for performing the SEM imaging and Abdel Khouhk for the ^{1}H NMR analysis and finally, Julien Rigolini and Gerald Clisson for their assistance in developing the MSEC technique.

REFERENCES

1 Taylor K.C., Nasr-El-Din H.A. (1998) *J. Phys. Chem. B* **19**, 265-280.

2 Taylor K.C., Nasr-El-Din H.A. (2007) Presented at *the Petroleum Society's 8th Canadian International Petroleum Conference*, Calgary, AB, Canada, 12-14 June, *paper CIPC 2007-016*.

3 Eoff L., Dalrymple D., Reddy B.R. (2005) *SPE Prod. Facil.* August, 250-256.

4 Feng Y., Billon L., Grassl B., Khoukh A., François J. (2001) *Polymer* **43**, 2055-2064.

5 Feng Y., Grassl B., Billon L., Khoukh A., François J. (2002) *Polym. Int.* **51**, 939-947.

6 Grassl B., Billon L., Borisov O., Francois J. (2006) *Polym. Int.* **55**, 1169-1176.

7 Paillet S., Grassl B., Khoukh A., Torres M., Desbrières J., Muller A.J. (2009) *Macromolecules* **42**, 13, 4914-4917.

8 Kujawa P., Audibert-Hayet A., Selb J., Candau F. (2004) *J. Polym. Sci.* **42**, 1640-1655.

9 Kujawa P., Audibert-Hayet A., Selb J., Candau F. (2006) *Macromolecules* **39**, 1, 384-392.

10 Cadix A., Chassenieux C., Lafuma F., Lequeux F. (2005) *Macromolecules* **38**, 2, 527-536.

11 Penott-Chang E.K., Gouveia L., Fernandez I.J., Muller A.J., Az-Barrios A., Saez A.E. (2007) *Colloid. Surface. A: Physicochem. Eng. Aspects* **295**, 99-106.

12 McCormick C.L., Johnson B. (1988) Structurally Tailored Macromolecules for Mobility Control in Enhanced Oil Recovery, in *Water-Soluble Polymers for Petroleum Recovery*, Stahl G.A., Schulz D.N. (eds), Plenum Press, New-York, NY, USA, pp. 161-180.

13 Bai G., Gonçalves C, Gama F.M., Bastos M. (2008) *Thermochimica Acta* **467**, 54-62.

14 Yamamoto H., Mizusaki M., Yoda K., Morishima Y. (1998) *Macromolecules* **31**, 3588-3594.

15 Sato Y., Hashidzume A., Morishima Y. (2001) *Macromolecules* **34**, 6121-6130.

16 Dutta P., Dey J., Ghosh G., Nayak R.R. (2009) *Polymer* **50**, 1516-1525.

17 Ye L., Li Q., Huang R. (2006) *J. Appl. Polym. Sci.* **101**, 2953-2959.

18 Zhao Y., Zhou J., Xu X., Liu W., Zhang J., Fan M., Wang J. (2009) *Colloid Polym. Sci.* **287**, 237-241.

19 Petit F., Illiopoulos I., Audebert R. (1998) *Polymer* **39**, 3, 751-753.

20 Fur I., Illiopoulos I., Stilbs P. (2000) *J. Phys. Chem. B* **104**, 3, 485-494.

21 Klucker R., Schosseler F. (1997) *Macromolecules* **30**, 4228-4231.

22 Beaudouin E., Borisov O., Lapp A., Billon L., Hiorns R.C., François J. (2002) *Macromolecules* **35**, 7436-7447.

23 Kim M., Choi Y.W., Sim J.H., Choo J., Sohn D. (2004) *J. Phys. Chem. B* **108**, 8269-8277.

24 Esquenet C., Terech P., Boue F., Buhler E. (2004) *Langmuir* **20**, 3583-3592.

25 Dai S., Tam K.C., Jenkins R.D. (2000) *Macromolecules* **33**, 404-411.

26 Dai S., Tam K.C., Jenkins R.D., Bassett D.R. (2000) *Macromolecules* **33**, 7021-7028.

27 Dai S., Tam K.C., Jenkins R.D. (2001) *Macromol. Chem. Phys.* **202**, 335-342.

28 Zhou Z., Peiffer D.G., Chu B. (1994) *Macromolecules* **27**, 1428-1433.

29 Zhou Z., Chu B., Nace V.M. (1996) *Langmuir* **12**, 5016-5021.

30 Zhou Z., Yang Y.W., Booth C., Chu B. (1996) *Macromolecules* **29**, 8357-8361.

31 Morishima Y., Nomura S., Ikeda T., Seki M., Kamachi M. (1995) *Macromolecules* **28**, 2874-2881.

32 Hashidzume A., Yamamoto H., Mizusaki M., Morishima Y. (1999) *Polym. J.* **31**, 1009-1014.

33 Yamamoto H., Morishima Y. (1999) *Macromolecules* **32**, 7469-7475.

34 Kawata T., Hashidzume A., Sato Y. (2007) *Macromolecules* **40**, 1174-1180.

35 Vidal R.R.L., Balaban R., Borsali R. (2008) *Polym. Eng. Sci.* 2011-2026.

36 Alami E., Almgren M., Brown W., François J. (1996) *Macromolecules* **29**, 2229-2243.

37 Wu S., Shanks R.A., Bryant G. (2006) *J. Appl. Polym. Sci.* **100**, 4348-4360.

38 Borisov O.V., Zhulina E.B. (2005) *Macromolecules* **38**, 6, 2506-2514.

39 Koga T., Tanaka F., Motokawa R., Koizumi S., Winnik F.M. (2008) *Macromolecules* **41**, 9413-9422.

40 Rubinstein M., Semenov A.N. (2001) *Macromolecules* **34**, 1058-1068.

41 Chhabra R.P., Comiti J., Machac I. (2001) *Chem. Eng. Sci.* **56**, 1-27.

42 Sury A., Machac I. (2009) *Chemical Papers* **63**, 2, 131-139.

43 Sorbie K.S. (1991) *Polymer-Improved Oil Recovery*, Blackie (ed.), CRC Press, Glasgow.

44 Chauveteau G., Sorbie K.S. (1991) Mobility Control by Polymers, in *Basic Concepts in Enhanced Oil Recovery Processes, in Critical reports on applied Chemistry*, Bavière M. (ed.), Elsevier Science Publishers, Vol. 33, pp. 43-87.

45 Chauveteau G. (1982) *J. Rheol.* **26**, 2, 111-142.

46 Lecourtier J., Chauveteau G. (1984) presented at *the SPE Annual Technical Conference and Exhibition*, Houston, Texas, 16-19 September, *SPE paper* 13034.

47 Bagassi M., Chauveteau G., Lecourtier J., Englert J., Tirrel M. (1989) *Macromolecules* **22**, 262-266.

48 Zitha P.L.J., Chauveteau G., Léger L. (2001) *J. Colloid Interface Sci.* **234**, 269-283.

49 Lu H., Feng Y, Huang Z. (2008) *J. Appl. Polym. Sci.* **110**, 1837-1843.

50 Maia A.M.S, Borsali R., Balaban R.C. (2009) *Mater. Sci. Eng. C Biomimetic Supramol Syst.* **29**, 2, 505-509.

51 Argillier J.-F., Audibert-Hayet A., Lecourtier J., Moan M., Rousseau L. (1996) *Colloids Surf. A: Physicochem. Eng. Aspects* **113**, 247-257.

52 Volpert E., Selb J., Candau F., Green N, Argillier J.F., Audibert A. (1998) *Langmuir* **14**, 1870-1879.

53 Kim H.S., Lau W., Kumacheva E. (2000) *Macromolecules* **33**, 4561-4567.

54 Wakeman R.J., Akay G. (1994) *J. Membr. Sci.* **91**, 145-152.

55 Akay G., Wakeman R.J. (1997) *J. Membrane Sci.* **131**, 229-236.

56 Kun R., Jinlan W, Meiqin L., Chunming X. (2006) *Petrol. Sci.* **3**, 2, 66-72.

57 Dupuis G., Rigolini J., Clisson G., Rousseau D., Tabary R., Grassl B. (2009) *Anal. Chem.* **81**, 8993-9001.

58 Candau F., Selb J. (1999) *Adv. Colloid Interface Sci.* **49**, 149-172.

59 Blagodatskikh I.V., Vasil'eva O.V., Ivanova E.M., Bykov S.V., Churochkina N.A., Pryakhina T.A., Smirnov V.A., Philippova O.E., Khokhlov A.R. (2004) *Polymer* **45**, 17, 5897-5904.

60 Berne B.J., Pecora R. (2000) *Dynamic Light Scattering with Applications to Chemistry, Biology, and Physics*, Dover Publications.

61 Bird R.B., Armstrong R.C., Hassager O. (1987) *Dynamics of Polymeric Liquids*, John Wiley & Sons, New York.

62 Moan M., Chauveteau G., Ghoniem S. (1979) *J. Non-Newton. Fluid Mech.* **5**, 463-474.

63 Van den Berg G.B., Smolders C.A. (1990) *Desalination* **77**, 101-133.

64 Sablani S.S., Goosen M.F.A., Al-Belushi R., Wilf M. (2001) *Desalination* **141**, 269-289.

65 Fernandez-Sempere J., Ruiz-Bevia F., Garcia-Algado P., Salcedo-Diaz R. (2009) *J. Membr. Sci.* **342**, 279-290.

66 Gouveia L., Paillet S., Khoukh A., Grassl B., Muller A.J. (2008) *Colloids Surf. A: Physicochem. Eng. Aspects* **322**, 211-218.

67 De Gennes P.G. (1979) *Scaling Concept in Polymer Physics*, Cornell University Press.

68 Argillier J.F., Audibert A., Lecourtier J., Moan M., Rousseau L. (1996) *Colloids Surf. A: Physicochem. Eng. Aspects* **113**, 247-257.

69 Rivenq R.C., Donche A., NoiK C. (1992) *SPE Reserv. Eng.* **7**, 1, 15-20.

70 Adam M., Lairez D. (1996) Sol-gel Transition, in *Physical Properties of Polymeric Gels*, Cohen-Addad J.P. (ed.), John Wiley & Sons, pp. 87-142.

71 Dupuis G., Rousseau D., Tabary R., Grassl B. (2011) *SPE J.* **16**, 1, 43-54, *SPE* 129884-PA.

Final manuscript received in March 2012
Published online in January 2013